Acta Geologica Sinica (English Edition), 2023, 97(1): 149–162

Single-element Anomaly Mapping from Stream Sediment Geochemical Landscapes Aided by Digital Terrain Analysis

XIANG Jie[1, 2], XIA Peng[1, 3, *], XIAO Keyan[4], Emmanuel John M. CARRANZA[5] and CHEN Jianping[6]

[1] *International Mining Research Center, China Geological Survey, Beijing 100037, China*
[2] *China Mining News, China Geological Survey, Beijing 100037, China*
[3] *Institute of Advanced Studies, China University of Geosciences, Wuhan 430074, China*
[4] *MNR Key Laboratory of Metallogeny and Mineral Resource Assessment, Institute of Mineral Resources, Chinese Academy of Geological Sciences, Beijing 100037, China*
[5] *Department of Geology, University of the Free State, Bloemfontein, South Africa*
[6] *School of Earth Sciences and Resources, China University of Geosciences, Beijing 100083, China*

Abstract: The identification of anomalies within stream sediment geochemical data is one of the fastest developing areas in mineral exploration. The various means used to achieve this objective make use of either continuous or discrete field models of stream sediment geochemical data. To map anomalies in a discrete field model of such data, two corrections are required: background correction and downstream dilution correction. Topography and geomorphology are important factors in variations of element content in stream sediments. However, few studies have considered, through the use of digital terrain analysis, the influence of geomorphic features in downstream dilution correction of stream sediment geochemical data. This study proposes and demonstrates an improvement to the traditional downstream dilution correction equation, based on the use of digital terrain analysis to map single-element anomalies in stream sediment geochemical landscapes. Moreover, this study compares the results of analyses using discrete and continuous field models of stream sediment geochemical data from the Xincang area, Tibet. The efficiency of the proposed methodology was validated against known mineral occurrences. The results indicate that catchment-based analysis outperforms interpolation-based analysis of stream sediment geochemical data for anomaly mapping. Meanwhile, the proposed modified downstream dilution correction equation proved more effective than the original equation. However, further testing of this modified downstream dilution correction is needed in other areas, in order to investigate its efficiency further.

Key words: stream sediment, sample catchment basin, digital terrain analysis, downstream dilution correction, background correction

Citation: Xiang et al., 2023. Single-element Anomaly Mapping from Stream Sediment Geochemical Landscapes Aided by Digital Terrain Analysis. Acta Geologica Sinica (English Edition), 97(1): 149–162. DOI: 10.1111/1755-6724.14992

1 Introduction

The identification of geochemical anomalies from stream sediment geochemical data provides significant information for mineral exploration, especially in the preliminary stages (Carranza and Hale, 1997; Cheng, 1999, 2007; Carranza, 2004; Zuo et al., 2013, 2015, 2009; Wang et al., 2014, 2018; Ghezelbash et al., 2019). In the past few decades, a variety of new mapping techniques have been developed and applied for stream sediment geochemical anomaly mapping (Stanley and Sinclair, 1989; Cheng, 1999, 2007; Carranza, 2004, 2010a; Yousefi et al., 2013; Mokhtari and Garousi Nezhad, 2015; Zuo et al., 2015; Kirkwood et al., 2016; Zuo, 2016, 2017; Zuo and Xiong, 2018; Parsa et al., 2018, 2017; Wang et al., 2018; Ghezelbash et al., 2019; Shahrestani et al., 2019; Ayari et al., 2022; Nforba et al., 2022; Ghasemzadeh et al., 2022). Anomalies in stream sediment geochemical data can be identified as either discrete or continuous fields (Carranza, 2008, 2010b), depending on whether or not the spatial representation of such data considers the geomorphological constraints of watersheds.

Continuous fields of stream sediment geochemical data are based on a variety of interpolation techniques, such as inverse distance weighting (IDW), kriging and the multifractal interpolation method (MIM). To distinguish anomalies from background levels in continuous-field stream sediment geochemical data, Cheng et al. (1994) proposed the concentration-area (C-A) fractal model in the spatial domain, whereas Cheng (1999) and Cheng et al. (2000) proposed the spectrum-area (S-A) multifractal model in the frequency domain. For identifying weak anomalies in continuous-field stream sediment geochemical data, local singularity analysis (LSA) was proposed by Cheng (2007) and demonstrated by Wang et al. (2018) and Zuo et al. (2009). Recently, a variety of machine learning and deep learning algorithms have been widely developed and applied to map geochemical

* Corresponding author. E-mail: xiapeng@mail.cgs.gov.cn

anomalies (He et al., 2022; Wu et al., 2022; Xiong and Zuo, 2022; Zhang et al., 2022).

The chemical compositions of stream sediments are, however, derived from weathering and the erosion of rocks and soil upstream in the catchment basin. Therefore, the above-mentioned interpolation-based techniques suffer from neglect of geomorphological and hydrodynamic considerations, or fail to account for transport and deposition processes. In this regard, many methods have been proposed for anomaly mapping in discrete field geochemical data. These methods include analyses by sample catchment basins (SCB) (Bonham-Carter and Goodfellow, 1984; Bonham-Carter et al., 1987; Carranza and Hale, 1997; Carranza 2008, 2010a, b; Abdolmaleki et al., 2014; Ghezelbash et al., 2019; Shahrestani et al., 2019; Najafian et al., 2020), stream orders (Carranza, 2004), extended sample catchment basins (ESCB) (Spadoni, 2006) and weighted drainage catchment basins (WDCB) (Yousefi et al., 2013; Farahbakhsh et al., 2019). In these methods, the value within each discrete field that is linked to each sample is the same, thus precluding 'mathematical interference' between neighboring samples (Lancianese and Dinelli, 2015).

For anomaly mapping in discrete fields of stream sediment geochemical data, two factors are considered, namely background correction and downstream dilution correction. Bonham-Carter et al. (1987) proposed the weighted average method, in order to estimate background concentration per element per lithological unit, which became the most widely-used method to estimate and remove the background contribution of lithology to elemental values in stream sediments. For downstream dilution correction after background correction, Hawkes (1976) proposed the most widely used and idealized formula (see Equation (1) below), which was a great achievement in the analysis and interpretation of stream sediment geochemical data (Carranza and Hale, 1997). Although later researchers have proposed modified downstream dilution-correction models (e.g., Mokhtari and Garousi Nezhad, 2015), the downstream dilution correction equation of Hawkes (1976) remains highly cited in research of geochemical anomaly mapping methods that take into consideration the stream sediment downstream dilution phenomenon. Abdolmaleki et al. (2014) considered slope effect and used 3D surfaces to improve the identification of anomalous catchment basins. However, although topography and geomorphology are factors in varying elemental contents in stream sediments, only a few studies have examined the influence of geomorphic features to provide a sophisticated downstream dilution correction method, based on digital terrain analysis.

In the last decade or so, there has been a dramatic increase in the range of techniques that involve topographic analyses, especially using high-resolution topographic data, which provide new insights to better understanding Earth's surface processes (Tarolli, 2014). A variety of geomorphic methods have been introduced, such as roughness index (Morris et al., 2008) and sediment connectivity index (Cavalli et al., 2013). These methods give us new opportunities for mapping stream sediment geochemical anomalies, based on digital terrain analysis.

The purpose of this study was to carry out a geomorphic analysis to improve downstream dilution correction and, thus, improve the recognition of stream sediment geochemical anomalies. This work compares the performance of methods for anomaly mapping from discrete and continuous fields of stream sediment geochemical data in the Xincang area in the southeast of Tibet. As a result of the plateau climate in this area, the vegetation cover is very scarce and so outcrops of bedrock are both abundant and widespread. Here, we improved the traditional downstream dilution correction equation, based on digital terrain analysis for single-element anomaly mapping from stream sediment geochemical data. The efficiency of these methods was validated against the known mineral occurrences in the area.

2 Geological Background and Data Collection

2.1 Geological setting

The study area, located in the eastern part of the southern Gangdese metallogenic belt, is a world-class Cu-polymetallic metallogenic belt between the Yarlung–Zangbo suture zone and the Bangong–Nujiang suture zone. The study area experienced tectonic evolution as follows: southward subduction of the Bangong–Nujiang ancient Tethys oceanic crust, formation of the Neo-Tethys Ocean, northward subduction of the Yarlung–Zangbo Neo -Tethys crust and the continental collision between the Indian continent and the Lhasa block (Pan et al., 2012). The study area has formed a complex tectonic pattern, mainly manifesting as regional E–W trending compressional faults, N–S trending tensional faults and NE to NW trending strike-slip faults (Leng et al., 2016).

The study area, measuring ~450 km^2, is encompassed by the 1: 50,000 scale geological map of Xincang (Fig. 1). The strata exposed in the area are mainly the first and second members of the Yeba, Duodigou and Linbuzong formations, which are overlain by Quaternary sediments. Outcrops of Late Cretaceous to Miocene biotite adamellite, granodiorite-porphyry and granite porphyry are distributed widely in the southern part of the study area. The known mineral deposit types in the area are mainly porphyry and skarn Cu-polymetallic deposits related to the Miocene intermediate-acidic hypabyssal magmatism (Qu et al., 2007).

2.2 Sampling and data collection

The Geological Survey Institute of Tibet has carried out high-density regional-scale sampling (1 sample per 1 km^2) by collecting 451 stream sediment samples in the study area. The data comprised concentrations of 13 elements (Au, Ag, Ba, Bi, Cd, Cu, Fe, Mo, Pb, Sb, Sn, W, Zn) in ppm, except Au (ppb) and Fe (%) (Table 1). The concentrations of these elements were determined by different analytical methods, with different detection limits (Table 2). Further details regarding laboratory sample preparation and the analysis of stream sediment element concentrations can be found in Xie et al. (1997, 2008).

The sampling sites were selected, based on analysis of a

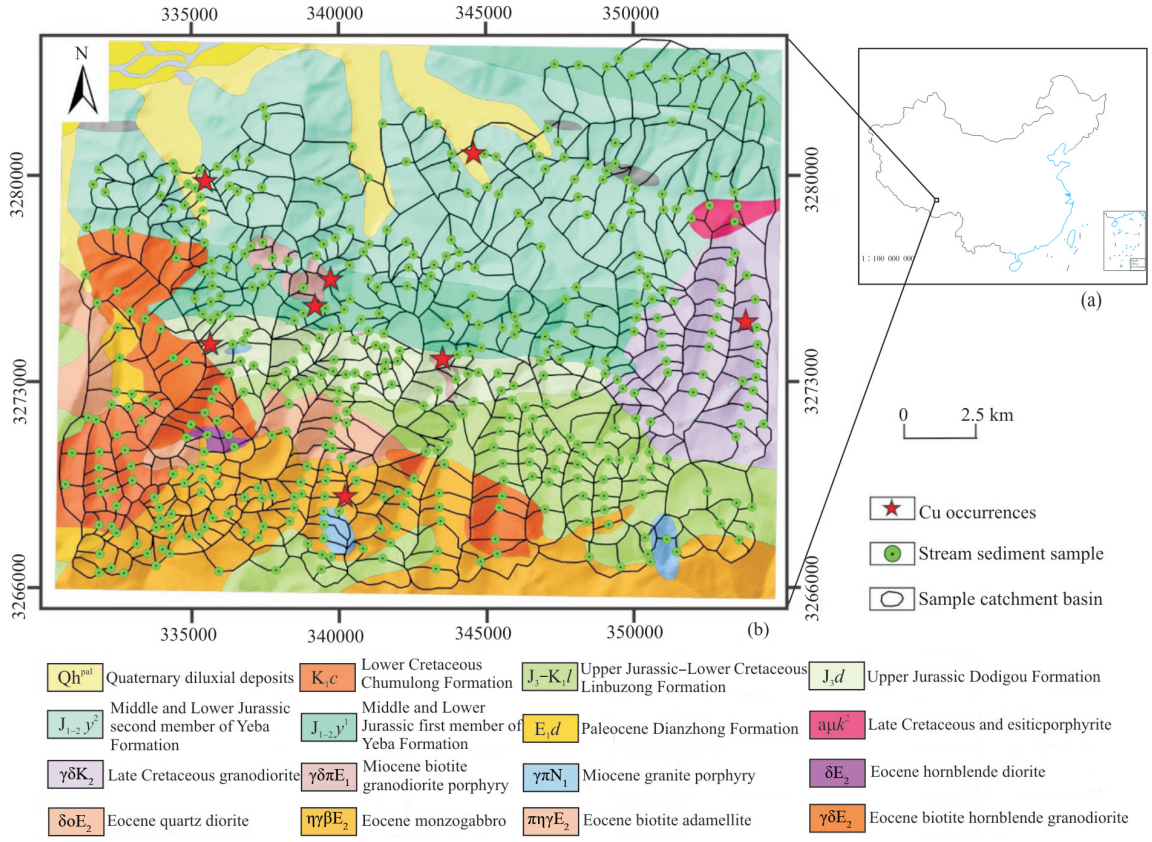

Fig. 1. (a) Location of the study area in the southwest of China; (b) simplified geological map showing the location of the samples and their related catchment basins. Lithological abbreviations are described in Table 3.

Table 1 Descriptive statistics of elemental values in stream sediment samples (N = 451)

Element	Min	P25	Median	p75	p95	Max	MAD	Mean	SD	CV (%)
Ag	0.019	0.073	0.108	0.141	0.25	0.71	0.035	0.122	0.08	65.502
Au (ppb)	0.31	1.04	1.58	2.43	4.946	20.8	0.65	2.057	1.897	92.22
Ba	312	413	434	461	507.2	684	23	438.042	42.717	9.752
Bi	0.11	0.45	0.52	0.63	0.864	3.22	0.09	0.578	0.284	49.034
Cd	0.025	0.091	0.12	0.17	0.324	1.43	0.034	0.152	0.115	75.634
Cu	6.36	19.1	23.9	29.3	43.72	938	5.1	28.441	47.664	167.589
Fe (%)	1.645	2.898	3.339	3.64	4.185	6.16	0.35	3.211	0.724	22.547
Mo	0.19	0.52	0.72	0.99	2.284	64.7	0.22	1.214	3.504	288.626
Pb	10.4	28.2	30.5	33.4	39.68	182	2.5	32.129	13.148	40.922
Sb	0.34	0.9	1.1	1.37	2.466	46.3	0.22	1.372	2.257	164.535
Sn	1.1	2.97	3.63	4.26	5.152	5.88	0.64	3.593	0.945	26.291
W	1.03	2.8	3.47	4.19	5.95	16.6	0.69	3.694	1.533	41.51
Zn	28.5	62.5	75.7	84.8	110.8	277	11.2	75.633	23.612	31.219

P = values at the 25th, 75th and 95th percentiles. SD = standard deviation. MAD = median of absolute deviation from median; CV = coefficient of variation. Concentrations are in ppm unless mentioned otherwise.

Table 2 Methods used and corresponding detection limits for analysis of 13 elements

Element	Analytical method	Detection limit (ppm)	Element	Analytical method	Detection limit (ppm)
Ag	ES	0.01	Mo	POL	0.1
Au	GS-AAS	1 ppb	Pb	XRF	0.2
Ba	XRF	0.2	Sb	HG-AFS	0.1
Bi	HG-AFS	0.05	Sn	ES	0.2
Cd	ICP-MS	0.01	W	POL	0.1
Cu	XRF	0.2	Zn	XRF	0.2
Fe	XRF	0.10%			

ES = emission spectrometry; GF-AAS = graphite furnace-atomic absorption spectrometry; XRF = X-ray fluorescence spectrometry; HG-AFS = hydride generation-atomic fluorescence spectrometry; ICP-MS = inductively coupled plasma-mass spectrometry; POL = polarography.

digital elevation model (DEM) of the study area. In this study, the DEM used was generated from digitized elevation contour lines (Ardiansyah and Yokoyama, 2002), which were part of the 1: 50,000 scale geological map of Xincang (Fig. 1). Elevations in the study area range from 3690 to 5620 m a.s.l. (average of 4640 m a.s.l.). Topographic slopes range between 0° and 63° (average 23°). Comparison of the values in this DEM with actual elevation data, which were measured using a dual-frequency RTK DGPS, gave a DEM bias of less than 5 m. Thus, this high-resolution DEM gives us new opportunities for better analysis of geomorphic features to support anomaly mapping from stream sediment geochemical data.

3 Methods

3.1 Catchment basin analysis

As mentioned above, stream sediments are mixtures of materials in a catchment basin. In order to map geochemical anomalies in stream sediment SCBs, lithology and downstream dilution phenomena should be taken into account in processing and analysing the data. Since the 1970s, many researchers studied different geochemical and geomorphic aspects of stream sediment samples, in order to quantify and correct the influence of lithological background and downstream dilution phenomena (Hawkes, 1976; Bonham-Carter et al., 1987; Spadoni, 2006; Mokhtari and Garousi Nezhad, 2015; Farahbakhsh et al., 2019; Najafian et al., 2020). However, the most highly cited research on downstream dilution of stream sediment chemical composition is the work by Hawkes (1976), who proposed the following equation to depict the relationship between element content (C_a) in a catchment (with area of A_a) and assumed anomalous element content (C_m) from a mineralized source with area of A_m:

$$C_a A_a = C_m A_m + C_b (A_a - A_m) \quad (1)$$

where C_b is background element content due to non-mineralized lithology, with a surface area of $A_a - A_m$ (Fig. 2). To remove background levels due to lithology, the C_b was estimated using the method proposed by Bonham-Carter et al. (1987). Firstly, the weighted mean element content M_j (j = 1, 2, …, m) contributed by the j-th lithological units was estimated as:

$$M_j = \sum_{i=1}^{n} C_i A_{ij} / \sum_{i=1}^{n} A_{ij} \quad (2)$$

where A_{ij} is the area of the j-th lithological unit in SCB (i = 1, 2, …, n). The local background element content (C_i') due to lithology was then estimated as:

$$C_i' = \sum_{j=1}^{m} M_j A_{ij} / \sum_{i=1}^{m} A_{ij} \quad (3)$$

Residual values (i.e., $C_i - C_i'$), which are either positive or negative, can be interpreted as enrichment or depletion, respectively. Dilution-corrected residuals of element content (C_d) were estimated as (Hawkes, 1976; Carranza and Hale, 1997):

$$C_d = 100 A_i (C_i - C_i') \quad (4)$$

Positive residuals are of interest in mineral exploration, because they may be due to mineralization.

3.2 Digital terrain analysis

The area factor applied in the above equations is planar (i.e., 2D). However, surface areas of lithological units and SCBs are not planar (i.e., 3D), especially in mountainous regions. Therefore, the existing method to correct for downstream dilution effect (i.e., Eq. 4) neglects consideration of geomorphology, which is a key issue in the study of sediment delivery along channel networks (Cavalli et al., 2013).

For catchments in mountainous regions, such as in the study area, the concept of sediment connectivity can be used for analysis of sediment transfer processes. This analysis represents the extent of connection that controls sediment transfer from upslope sources to downslope

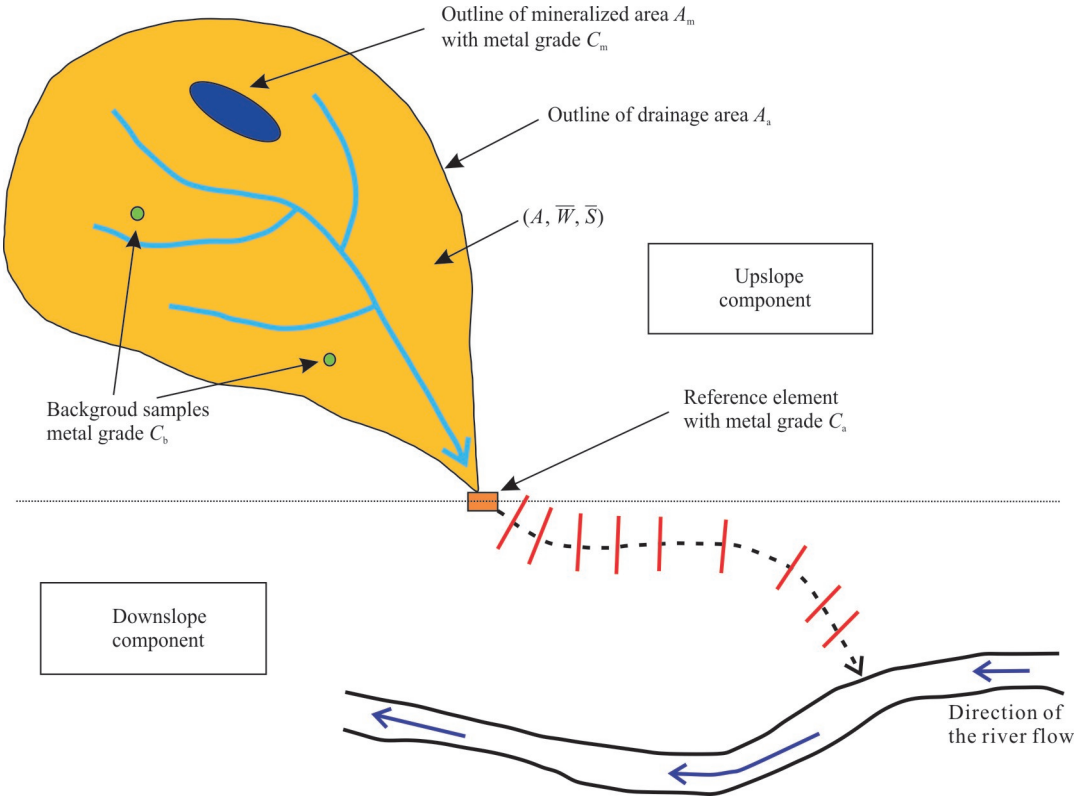

Fig. 2. Upslope and downslope components of the sediment connectivity index in an idealized catchment basin with mineralized and background (i.e., non-mineralized) rocks.

depositional areas. The index of sediment connectivity (*IC*), which was proposed by Borselli et al. (2008), provides a convenient tool with which to estimate potential linkages in the stream network, based on consideration of land use and topographic characteristics. The *IC* can be calculated as:

$$IC = \lg(\frac{D_{up}}{D_{dn}}) \quad (5)$$

where D_{up} and D_{dn} are the upslope and downslope components of connectivity, respectively (Fig. 2). The D_{up} represents the defluent potential for sediments, which are produced in upslope source areas. The D_{dn} refers to the flow path length that sediments must travel until they arrive at the neighboring features of interest.

For a better analysis of the downstream dilution effect, we focused on the defluent potential for upslope sediments, the D_{up} being estimated as:

$$D_{up} = \overline{WS}\sqrt{A} \quad (6)$$

where A refers to the upslope contributing area (m^2), with $\overline{W}$ and $\overline{S}$ representing the mean weighting factor and mean slope gradient (m/m) of the upslope contributing area, respectively.

3.3 Weighting factor

Cavalli et al. (2013) improved the IC method by introducing advanced methods of digital terrain analysis, such as the roughness index (*RI*) and multiple flow D-infinity approach. The *RI*, proposed by Cavalli and Marchi (2008), is determined as the standard deviation of residual topography (Fig. 3a), which is calculated as the difference between the original DEM and a smoothed version, derived by averaging DEM values in a moving window of n × n cells. Thus, the RI is estimated as:

$$RI = \sqrt{\frac{\sum_{i=1}^{n^2}(x_i - x_m)^2}{n^2}} \quad (7)$$

where n^2 is the number of cells within a moving window of n × n cells, x_i refers to the value of residual topography in a specific cell and x_m is the average value in n × n cells.

In addition, Borselli et al. (2008) proposed a weighting factor (*W*) to represent impedance to drainage and sediment transfer due to characteristics of Earth's surface (such as vegetation cover, surface lithology, particle size). As little vegetation cover exists in the study area, due to the high altitude and cold weather, the *RI* can act as a good proxy for the surface characteristics. Thus, using *RI*, the *W* can be calculated as:

$$W = 1 - (\frac{RI}{RI_{MAX}}) \quad (8)$$

where RI_{MAX} is the maximum *RI* value in the whole study area.

3.4 Contributing area

The original IC calculates the contributing area through the algorithm of single flow direction. In contrast, the upslope contributing area in the improved IC model is determined using the multiple flow direction D-infinity approach (Tarboron, 1997). In order to specify the flow direction, the earliest and simplest method (known as the D8 algorithm) assigns flow from each pixel into one of its eight neighbors, the upslope contributing area being estimated as the product of the pixel area and the number draining through pixels (Fig. 3b). For the D-infinity approach, the flow direction is decided by the steepest downward slope on planar triangular facets on a block-centered grid (Tarboron, 1997). The D8 algorithm results in a grid bias, due to restriction to eight possible flow directions. The traditional multiple flow direction method results in unrealistic over-dispersion, due to proportional flow. By contrast, the D-infinity approach has the great advantage that it is more robust than prior procedures based on fitting local planes while retaining a simple grid-based structure.

3.5 Modified equations of downstream dilution correction

To correct for the slope effect on downstream dilution, the 2D planar area of a SCB is replaced by a 3D surface area in Eqs. (2) and (3), the modified equations being, respectively:

$$M_{(3D)j} = \sum_{i=1}^{n} C_i A_{(3D)ij} / \sum_{i=1}^{n} A_{(3D)ij} \quad (9)$$

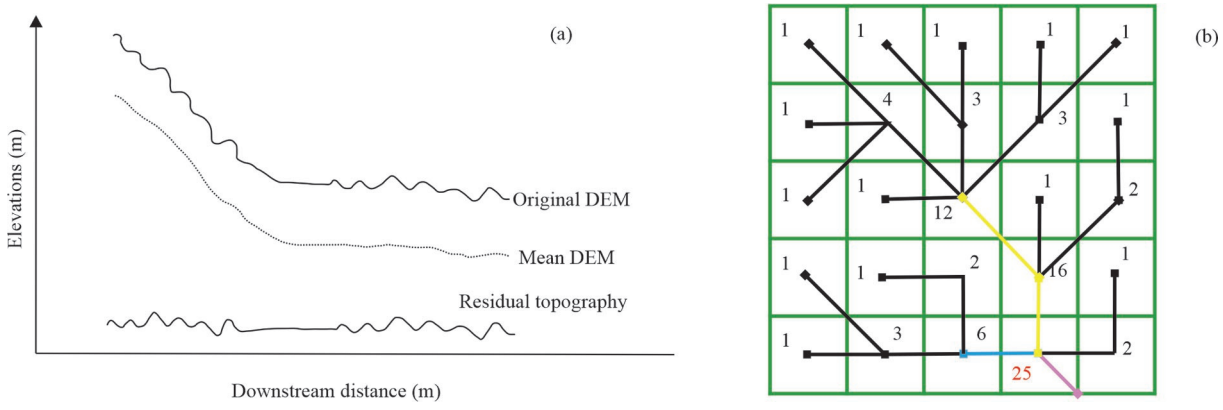

Fig. 3. Schematic illustration of (a) roughness index and (b) contributing area.

$$C'_{(3D)i} = \sum_{j=1}^{m} M_{(3D)j} A_{(3D)ij} / \sum_{i=1}^{m} A_{(3D)ij} \quad (10)$$

where $M_{(3D)j}$, $A_{(3D)ij}$, and $C'_{(3D)j}$ have the same meaning as in Eqs. (2) and (3), respectively, but in three dimensional space. Regarding the downstream dilution phenomenon, a coefficient K was developed to represent the potential of sediments produced upslope, the new equation for downstream dilution-corrected residuals of element contents (C_{nd}) being:

$$C_{nd} = 100 A_{(3D)i} \left(C_i - C'_{(3D)i} \right) K \quad (11)$$

where K can be set as 1, 0.75, 0.5 or 0.25, according to the D_{up}. In other words, the D_{up} values of sample catchment basins are sorted from largest to smallest and, if a SCB belongs to the top quartile based on its D_{up} values, the K of that basin is set as 1, whereas if a SCB belongs to the bottom quartile based on its D_{up} values, its K is set as 0.25.

3.6 Model evaluation

Over the past few decades, several fractal/multifractal models have been proposed for geochemical anomaly mapping. These methods include the concentration-area (C-A) fractal model (Cheng et al., 1994), spectrum-area (S-A) multifractal model (Cheng, 1999), concentration-distance (C-D) fractal model (Li et al., 2003), multifractal singularity analysis (Cheng, 2007) and the concentration-volume (C-V) fractal model (Afzal et al., 2011). In this study, the C-A method was used to establish thresholds for identification of stream sediment anomalies, because the thresholds are primarily used for discrete field models. A log-log plot of element concentration versus area with concentration values greater than a certain value was mapped, the thresholds for mapping geochemical anomalies being represented by breaks in lines fitted to the plot by least-squares regression (Cheng et al., 1994).

In this study, one continuous field model (derived by IDW interpolation) and five discrete field models were prepared, including measured metal content (MMC), background-corrected residuals in 2D (2DR), background-corrected residuals in 3D (3DR), dilution-corrected residuals (DCR) and revised dilution-corrected residuals (RDCR). To assess and compare the performance of these models in mapping geochemical anomalies, prediction-area (P-A) plots were used (Yousefi and Carranza, 2015). Firstly, two curves, one for cumulative occupied area and the other for probability of known mineralized occurrences, were plotted against threshold values. The normalized density (*ND*) could then be found at the point where these two curves intersect, the value of *ND* being represented as:

$$ND = \frac{P}{A} \quad (12)$$

where P refers to the prediction rate and A refers to the occupied area. The higher the *ND*, the higher the efficiency of geochemical anomaly mapping. Considering that most of the known mineralized occurrences are Cu mines, Cu alone was used as the element for testing the proposed methodology.

4 Results

4.1 Digital terrain analysis

Fig. 4 shows the results of digital terrain analysis of the study area in continuous and discrete fields. It is clear that the resulting continuous field models depict more details than the discrete field models; the latter is calculated by means of pixel values within the SCBs. Slopes in the study area range from 0° to 63° and the main distribution interval is 20° to 40°. Steep slopes are located mainly in the central parts of the study area and in the northwest part of the study area, near the Lhasa River (Fig. 4a, b). The values of *RI*, acting as impedance to stream flow, varied from 0 m to 1.2 m and ranged mainly from 0.4 m to 0.8 m. In the continuous field model, ridges and other topographic highs have higher *RI* values than valleys and other topographic lows (Fig. 4c). However, this topographic textural characteristic was suppressed completely in the discrete field model, which showed similar spatial structures to the slope (Fig. 4d). Both continuous and discrete field models of contributing area showed higher values along the channel network than along ridges (Fig. 4e, f), the contributing areas of the SCBs increasing with increasing stream order. This result is consistent with the fact that the contributing area of each grid cell was its own contribution plus the contribution from upslope neighboring cells. The values of D_{up} showed a somewhat similar spatial distribution to the contributing areas (Fig. 4g, h).

Thus, digital terrain analysis offers a better understanding of Earth's surface processes for the transport and deposition of stream sediments in the study area. The mean slope was then used to calculate the 3D surface area of each SCB. Finally, the D_{up} was used to rank every SCB's potential for downward routing of sediment formed upslope, the K being determined in order to adjust the magnitude of stream sediment downstream dilution, according to this order.

4.2 Sample catchment basin analysis

Table 3 indicates the background concentrations of Cu per lithological unit, based on 2D planar area and 3D surface area. There are no huge differences between background Cu concentrations within the same lithological unit when 2D planar areas and 3D surface areas are used; however, the values of Cu for different lithologies varied widely. The M_j values of Cu range from 17.89 to 99.88 ppm, the $M_{(3D)j}$ values of Cu varying between 17.68 and 101.02 ppm. The biotite granodiorite porphyry ($\gamma\delta\pi N_1$), limestone and mudstone (J_3d) have the highest M_j (or $M_{(3D)j}$) values of 99.88 ppm (101.02 ppm) and 54.82 ppm (55.17 ppm), respectively. In contrast, the sandy conglomerate and basaltic andesite (E_1d), quartz sandstone and conglomerate (J_3–K_1l) have the lowest M_j (or $M_{(3D)j}$) values of 17.89 ppm (17.68 ppm) and 18.33 ppm (18.38 ppm), respectively. For the other lithological units, the M_j (or $M_{(3D)j}$) values ranged from 20.05 ppm (20.03 ppm) to 30.81 ppm (31.01 ppm) (Table 3).

According to Taylor (1964), the Clarke value of Cu is 55 ppm, most of the lithological units in the study area having M_j (or $M_{(3D)j}$) values that are less than this Clarke

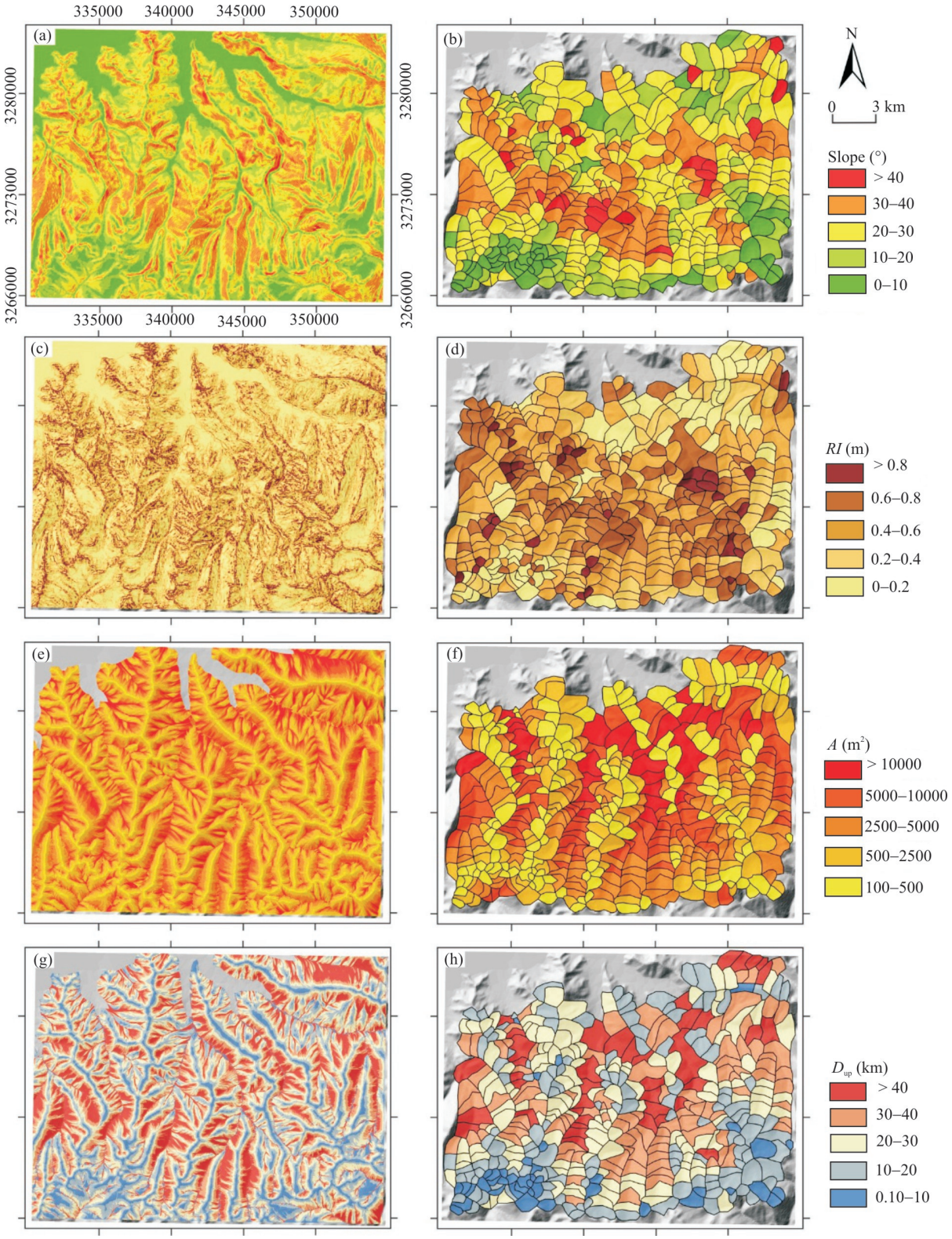

Fig. 4. Results of digital terrain analysis of the study area portrayed as continuous fields (left panel) and discrete fields (right panel): (a) slope; (b) mean slope; (c) roughness index; (d) mean roughness index; (e) contributing area; (f) mean contributing area; (g) upslope component D_{up}; (h) mean D_{up}.

value. The known occurrences of Cu mineralization in the study area are closely associated with the biotite granodiorite porphyry ($\gamma\delta\pi N_1$); this lithological unit has the highest M_J (or $M_{(3D)J}$) value. This result is consistent

Table 3 Background concentration of Cu per lithological unit, based on 2D planar area and 3D surface area (concentrations are in ppm)

Lithological unit	Description	M_j	$M_{(3D)j}$
Q_{hpal}	Brown gravel, sand gravel, clay	26.30	26.24
K_1c	Quartz sandstone, siltstone	26.80	26.86
J_3–K_1l	Quartz sandstone, conglomerate	18.33	18.38
J_3d	Limestone and mudstone, siltstones	54.82	55.17
J_1-2Y2	Tuff, andesite, dacite, sandstone, limestone, siliceous rock	27.36	27.33
J_1-2Y1	Volcanic breccia, agglomerate, siliceous rock	28.00	27.95
E_1d	Sandy conglomerate, basaltic andesite	17.89	17.68
$\alpha\mu K_2$	Andesitic porphyrite	28.51	28.54
$\gamma\delta K_2$	Granodiorite	22.11	22.27
$\gamma\delta\pi N_1$	Biotite granodiorite porphyry	99.88	101.02
$\gamma\pi N_1$	Granite porphyry	20.05	20.03
δE_2	Hornblende diorite	26.79	26.81
δoE_2	Biotite hornblende quartz diorite	29.17	29.02
$\eta\gamma\beta E_2$	Medium-fine grained biotite adamellite	30.81	31.01
$\pi\eta\gamma E_2$	Biotite adamellite	28.89	28.90
$\gamma\delta E_2$	Biotite hornblende granodiorite	28.88	28.88

with the metallogeny proposed by previous studies; that is, porphyry-type Cu deposits in the study area are genetically associated with late orogenic granitic porphyries emplaced during the late Himalayan epoch (Qu et al., 2007).

Fig. 5 shows the log-log plots of C-A models, based on IDW-interpolation of the Cu data and those created from SCB representation of the Cu data. A C-A log-log plot was obtained by plotting element concentration (C) versus area (A) occupied by concentration values greater than C. Five lines were fitted to the C-A models by using least-squares regression. The four break points along the fitted lines represent thresholds for classification of geochemical data (Table 4). Thus, five geochemical classes were defined: background levels (class 1), weak anomaly (class 2), moderate anomaly (class 3), anomaly (class 4) and strong anomaly (class 5).

As indicated in Fig. 5 and Table 4, there are similarities and differences among the C-A plots and thresholds. The Cu_{IDW} and the Cu_{MMC} yielded very similar C-A plots and thresholds, except for the values of threshold 4 (66 ppm for the Cu_{IDW} and 46.5 ppm for the Cu_{MMC}), which were used to map strong anomalies. For the background-corrected residuals, the thresholds obtained were very similar for the analysis using 2D planar area and 3D surface area. The likely reason for this is that the average slope (about 23°) in the study area was not very steep. For the dilution-corrected residuals and their corresponding revised dilution-corrected residuals, the thresholds obtained were strikingly different, but of the same order of magnitude.

Based on the thresholds given in Table 4, the maps of multi-class Cu geochemical anomalies are shown in Fig. 6. Overall, the southeastern part of the study area has the lowest Cu concentration, as reflected in all six maps. Based on the simplified geological map (Fig. 1b), the lithological units in the southeastern part of the study area (mainly J_3–K_1l, consisting of quartz sandstone and conglomerate) are associated with the second lowest background concentration of Cu (Table 3). Based on the maps of background-corrected residuals, the spatial distribution of Cu shows a high degree of aggregation. Strong anomalies are distributed primarily in the central part of the area, weak anomalies in the northern parts and moderate anomalies mainly in the southern parts (Fig. 6c, d). The spatial distribution of Cu is dispersed as shown in the other maps, especially the SCB maps.

As a reference for comparison of the maps, all of the known mineral occurrences and parts of the SCBs are labeled with numbers. Based on Fig. 6 and Table 5, only occurrence #7 (i.e., the large scale Qiangdui Cu deposit) was associated with a strong anomaly in all maps. Occurrence #8, which is the medium-sized Ganggari Cu (Mo) deposit, was mapped as a strong anomaly in all except the IDW-interpolated map. Occurrence #5 (i.e., the large-sized Lakange Cu (Mo) deposit) coincides with an anomaly or strong anomaly in all maps. Occurrences #1 and #2 map as a weak anomaly in Fig. 6a–d, but as an anomaly in Fig. 6e, f. Occurrences #3 and #4 correspond to a relatively strong anomaly in Fig. 6a, b, e, f; however, they correspond with a weak anomaly (as well as background levels) in Fig. 6c, d. In contrast, occurrence #6 coincides with a moderate anomaly in the IDW-interpolated map, an anomaly in Fig. 6b–d, but background levels in Fig. 6e, f.

The SCB 100 consists of lithological units Q_{hpal} and J_1-2Y2 with moderate M_j (or $M_{(3D)j}$) values (Table 3), which are close to the outlet of the main drainage. This means that SCB 100 is greatly influenced by the stream sediment downstream dilution phenomenon. Based on Fig. 6 and Table 5, SCB 100 is classified as a strong anomaly in the Cu_{DCR} and Cu_{RDCR} maps, but as background, weak anomaly and moderate anomaly in the Cu_{3DR}, Cu_{2DR} and Cu_{MMC} maps, respectively. Similarly, the SCBs 200 and 300 are classified as strong anomalies in the Cu_{DCR} and Cu_{RDCR} maps, but as relatively weak anomalies or background levels in the Cu_{3DR} and Cu_{2DR} maps. These SCBs may contain Cu mineralization or a related alteration and so should be investigated further through fieldwork.

4.3 Ability of the model to map anomalies

A high-quality stream sediment geochemical anomaly map can be a robust guide for mineral exploration, especially in the preliminary stages helping to narrow down the target areas. Therefore, a stream sediment geochemical anomaly map that delineates relatively small strong anomaly zones with a relatively high percentage of known mineral occurrences can be considered a high-quality anomaly map. Fig. 7 shows the P-A plots for the maps derived from all the aforementioned geochemical models. Overall, the defined thresholds are directly correlated with the percentage of known mineral occurrences (Table 6) and are inversely related to the occupied areas. These P-A plots display three pairs of maps with similar characteristics (Cu_{IDW} and Cu_{MMC}, Cu_{2DR} and Cu_{3DR}, Cu_{DCR} and Cu_{RDCR}), which are consistent with the spatial distribution characteristics in Figs. 5 and 6.

Table 6 shows the number of occurrences mapped per pre-defined threshold value. Only the maps of Cu_{IDW} and

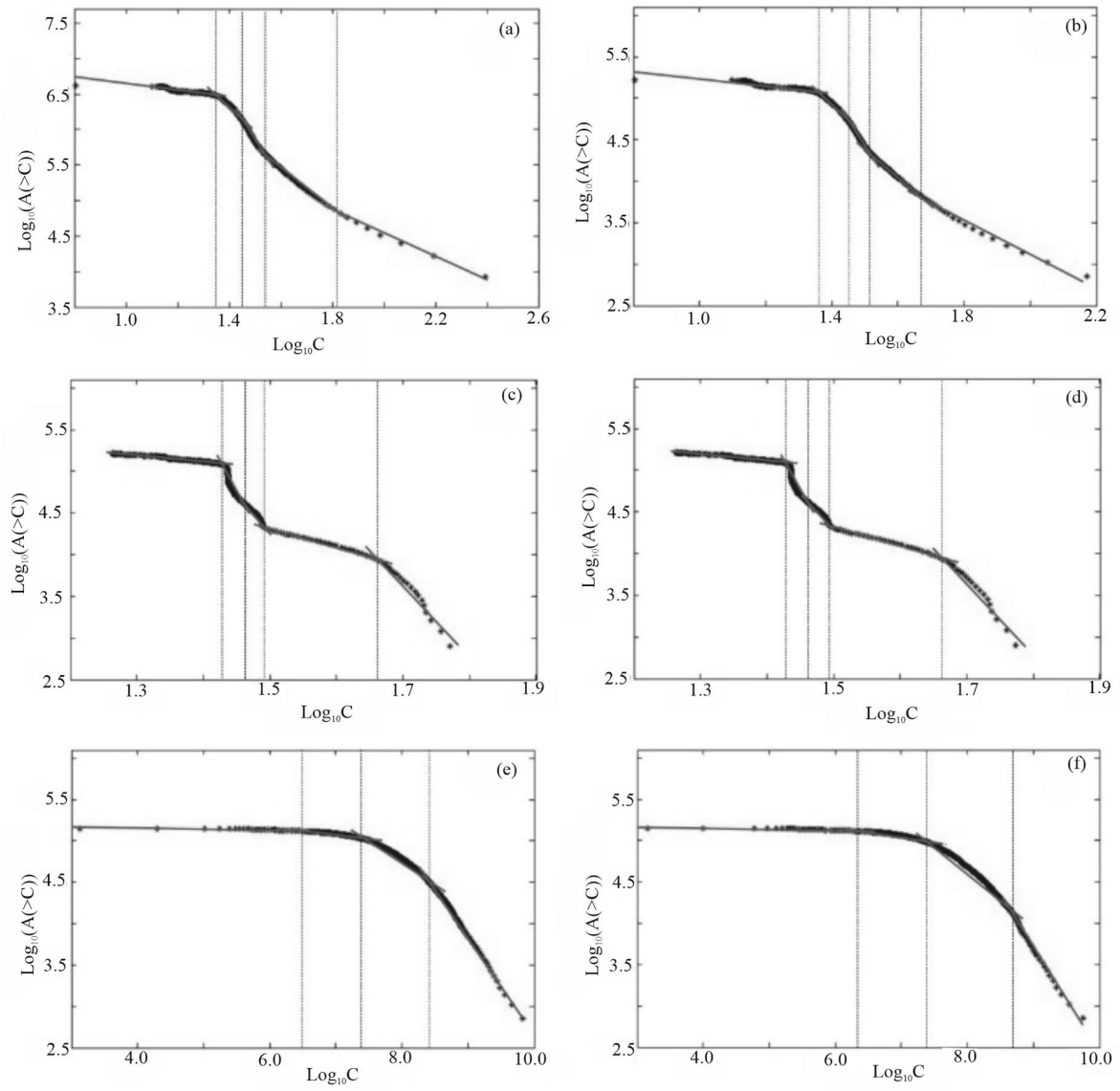

Fig. 5. Log-log plots of C-A models for (a) IDW-interpolated data; (b) measured metal content; (c) background-corrected residuals in 2D; (d) background-corrected residuals in 3D; (e) dilution-corrected residuals and (f) revised dilution-corrected residuals.

Table 4 Thresholds obtained by C-A modeling for classification of geochemical data

	Cu_{IDW}	Cu_{MMC}	Cu_{2DR}	Cu_{3DR}	Cu_{DCR}	Cu_{RDCR}
Threshold 1	22.3	23.0	26.7	26.9	0	0
Threshold 2	28.9	28.1	29.0	28.3	3507259	2317909
Threshold 3	34.8	32.3	31.0	31.3	35420161	27817973
Threshold 4	66.0	46.5	46.1	46.1	311584623	455468392

Cu_{MMC} delineated all of the occurrences as anomalies; the other maps delineated one occurrence as background levels. However, as the thresholds increased, the maps of dilution-corrected residuals (Cu_{DCR} and Cu_{RDCR}) have the highest percentage of known occurrences, whereas the maps of background-corrected residuals have the lowest percentage of known occurrences. These findings indicate that applying only background correction to stream sediment geochemical data is not enough for geochemical anomaly mapping and that areas defined by higher threshold values have higher prospecting probability for success.

Table 7 shows the *ND* values for the IDW, MMC, R and DCR methods extracted from the P-A plots (Fig. 7). The maps of Cu_{IDW} and Cu_{MMC}, Cu_{2DR} and Cu_{3DR}, Cu_{DCR} and Cu_{RDCR} yielded *ND* values of 2.23, 3.17, 1.60, 1.74, 4.35 and 6.62, respectively. Thus, the Cu_{RDCR} map has the highest *ND* value, reflecting that the revised downstream dilution-correction model has the best performance for geochemical anomaly mapping. The traditional Cu_{DCR} map yields the second highest *ND* value, demonstrating that downstream dilution correction is essential for mapping stream sediment geochemical anomalies. Comparing the Cu_{IDW} and Cu_{MMC} maps proves that SCB representation of stream sediment geochemical data can provide considerable improvement in anomaly mapping. However, the Cu_{2DR} map has the lowest ND value, followed by the Cu_{3DR} map. This further confirms that

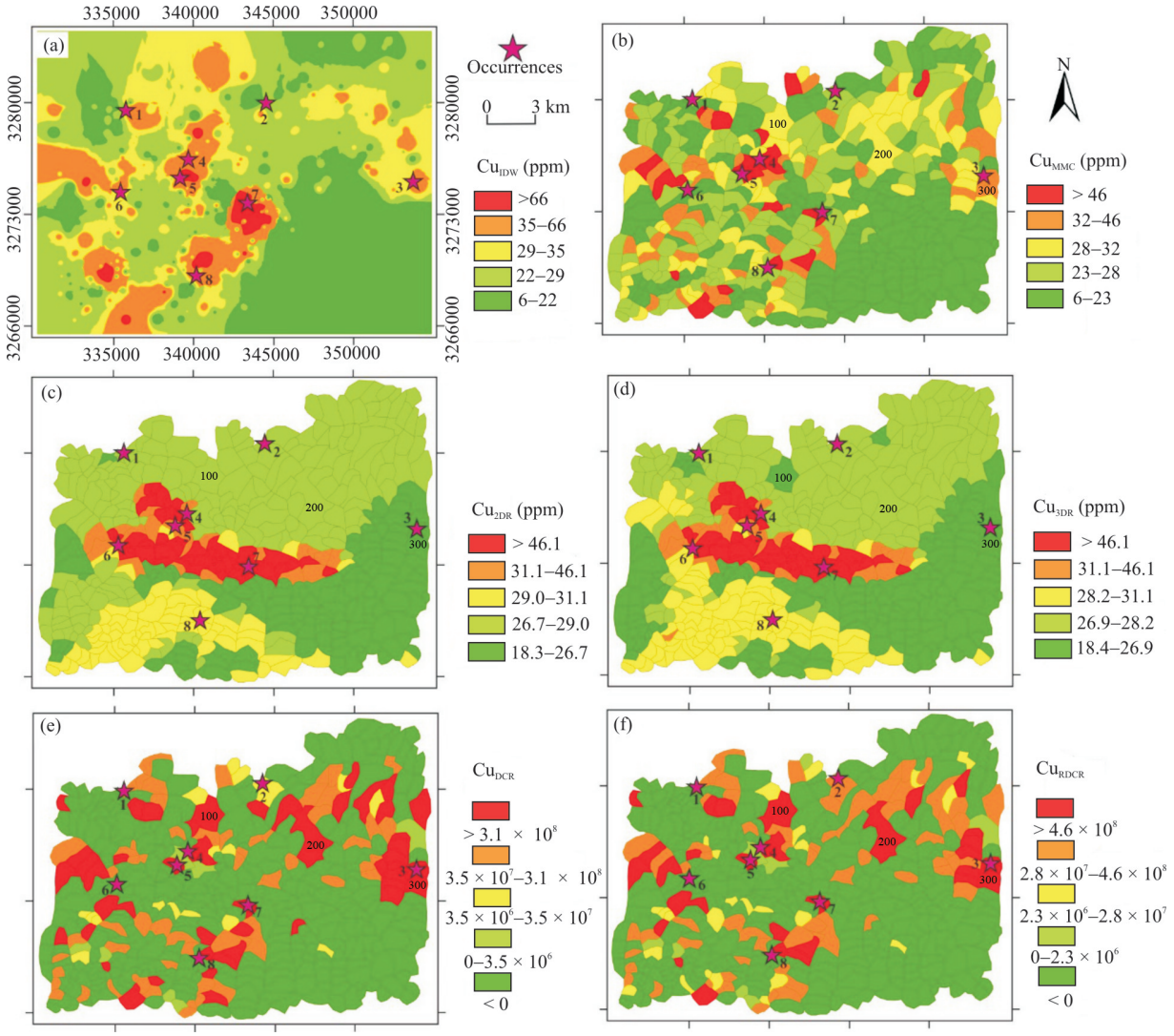

Fig. 6. Comparison of results of the different methods for identifying stream sediment geochemical anomalies: (a) Cu_{IDW}; (b) Cu_{MMC}; (c) Cu_{2DR}; (d) Cu_{3DR}; (e) Cu_{DCR}; (f) Cu_{RDCR}.

Table 5 Mineral occurrences, sample catchment basins and associated anomaly classes in different maps (Fig. 6)

Category	No.	Cu_{IDW}	Cu_{MMC}	Cu_{2DR}	Cu_{3DR}	Cu_{DCR}	Cu_{RDCR}
Mineral occurrences	1	Weak anomaly	Weak anomaly	Weak anomaly	Weak anomaly	Anomaly	Anomaly
	2	Weak anomaly	Weak anomaly	Weak anomaly	Weak anomaly	Moderate anomaly	Anomaly
	3	Anomaly	Anomaly	Background	Background	Strong anomaly	Strong anomaly
	4	Anomaly	Strong anomaly	Weak anomaly	Strong anomaly	Strong anomaly	Strong anomaly
	5	Anomaly	Strong anomaly	Anomaly	Anomaly	Strong anomaly	Strong anomaly
	6	Moderate anomaly	Anomaly	Anomaly	Anomaly	Background	Background
	7	Strong anomaly	Strong anomaly	Strong anomaly	Strong anomaly	Strong anomaly	Strong anomaly
	8	Anomaly	Strong anomaly	Strong anomaly	Strong anomaly	Strong anomaly	Strong anomaly
Sample catchment basins	100		Moderate anomaly	Weak anomaly	Background	Strong anomaly	Strong anomaly
	200		Moderate anomaly	Weak anomaly	Weak anomaly	Strong anomaly	Strong anomaly
	300		Anomaly	Background	Background	Strong anomaly	Strong anomaly

applying only background correction to stream sediment geochemical data is not enough for geochemical anomaly mapping in the study area. In addition, comparison of the Cu_{2DR} and Cu_{3DR} maps demonstrate that, in catchment basin analysis of stream sediment geochemical data, using 3D surface area for downstream dilution correction should be employed in preference to using 2D planar area.

5 Discussion

As stream sediments are a mixture of materials derived from rocks and soil from upstream/upslope of a sample location, there are a variety of factors that affect the variations in their elemental content. Those factors can be climatic, anthropogenic, sedimentological, lithological and

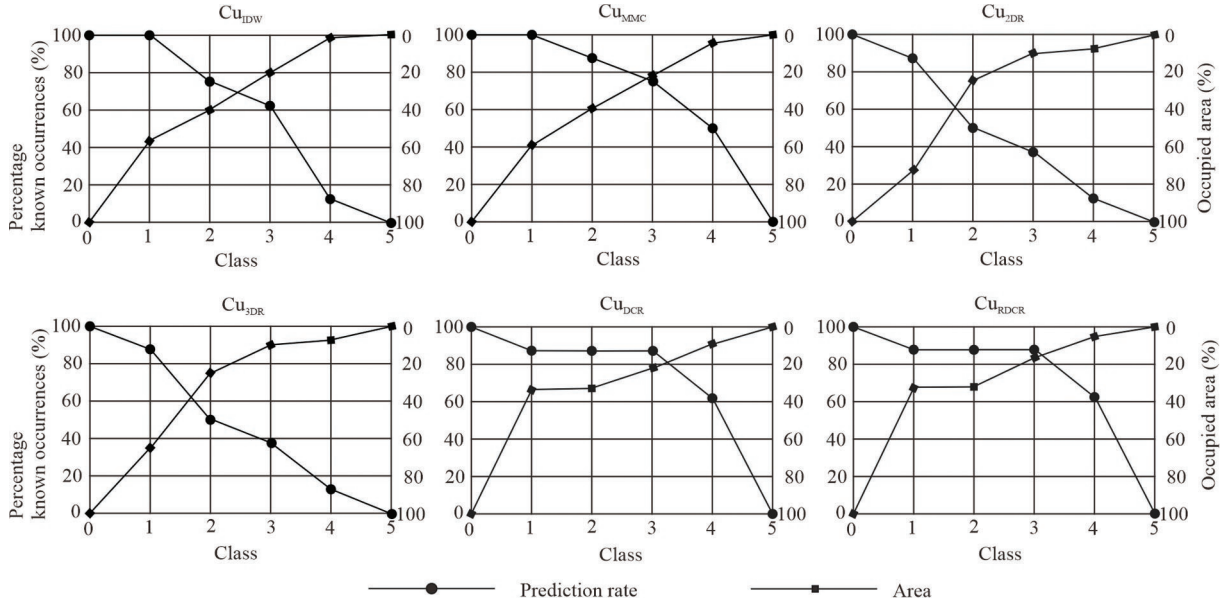

Fig. 7. Prediction-area plots for maps derived from IDW, MMC, 2DR, 3DR, DCR and RDCR methods.

Table 6 Number of mineral occurrences, delineated by threshold value

	Cu_{IDW}		Cu_{MMC}		Cu_{2DR}		Cu_{3DR}		Cu_{DCR}		Cu_{RDCR}	
	N	%	*N*	%	*N*	%	*N*	%	*N*	%	*N*	%
Class 0	8	100	8	100	8	100	8	100	8	100	8	100
Class 1	8	100	8	100	7	87.5	7	87.5	7	87.5	7	87.5
Class 2	6	75	7	87.5	4	50	4	50	7	87.5	7	87.5
Class 3	5	62.5	6	75	3	37.5	3	37.5	7	87.5	7	87.5
Class 4	1	12.5	4	50	1	12.5	1	12.5	5	62.5	5	62.5
Class 5	0	0	0	0	0	0	0	0	0	0	0	0

Table 7 Normalized density (*ND*) values for the IDW, MMC, R and DCR methods extracted from the P-A plots

Maps	Prediction map (%)	Occupied area (%)	Normalized density
Cu_{IDW}	69.04	30.96	2.23
Cu_{MMC}	76.03	23.97	3.17
Cu_{2DR}	61.53	38.47	1.60
Cu_{3DR}	63.55	36.45	1.74
Cu_{DCR}	81.31	18.69	4.35
Cu_{RDCR}	86.88	13.12	6.62

geomorphological factors. Some factors are random and difficult to quantify, but some factors are universal and important (e.g., lithological and geomorphological factors) and should not be ignored.

The lithological factor represents the main factor of sediment source and variation of elemental concentration. Estimation and removal of background elemental concentration due to lithology is key to recognition of significant geochemical anomalies (i.e., those related to mineral deposits). However, the traditional background correction and downstream dilution correction are clearly inadequate for identification of geochemical anomalies in stream sediment geochemical data, as confirmed in this study (Fig. 7; Table 7). Besides lithological factors, variation in elemental content in stream sediments is influenced by erosion and sediment deposition. Thus, in any area, geomorphological factors of stream sediment elemental composition involve mainly erosional and depositional processes, which are related to surface water flow.

The geomorphological factors are elucidated by the following three relationships: (i) catchment basins with steeper slopes are likely to have higher sediment erosion rate and lower sediment deposition rate; (ii) catchment basins with lower stream order usually have a higher sediment erosion rate and a lower sediment deposition rate (Carranza, 2004) and the contributing area can serve as a proxy for stream order; (iii) surface roughness of a catchment basin, which can impede water flow, can affect the rate of sediment erosion and the rate of sediment deposition. Accordingly, considering the developments in digital terrain analysis, we here introduce the concept of sediment connectivity to quantify the influence of geomorphological factors on variation in element content in stream sediments. This method provides a basic framework for quantifying geomorphological factors, opening the door to an improved understanding of the underlying drivers and the nature and degree of their ability to impact the variations in elemental content. Upslope components of connectivity analysis provide for comprehensive and accurate insight on the above-mentioned three relationships. From Equation (6), a catchment basin with higher D_{up} is likely to have steeper slopes, a larger contributing area, or lower surface roughness (or all of these). In addition, incorporation of slope effect allows for a better representation of surface area, which is more advantageous than planar area for downstream dilution correction in a mountainous region.

However, as different lithologies have different

weathering resistance, the original method of estimating the weighted mean concentration due to lithology (M_j), therefore, needs to be improved; this is because it merely considers the area occupied by each lithological unit in a catchment basin. Resistance to weathering by different lithological units should be taken into account. Here, we used the roughness index as a proxy for weathering resistance to estimate a weighting factor (W). Although the roughness index reflects impedance to runoff and sediment fluxes, which needs to be accounted for because the study area is located in the Tibetan Plateau with little vegetation cover, it can be used as a proxy for weathering resistance. That is, high surface roughness reflects stronger resistance to weathering, whereas lower surface roughness reflects a weaker resistance to weathering. For analysis of upslope components of connectivity in areas with dense vegetation cover, it may be better to use the C-factor of USLE-RUSLE models as a weighting factor (Renard et al., 1997), but this still needs to be demonstrated. In the last decade, a range of new techniques, such as light detection and ranging (LiDAR), among others, has led to a dramatic increase in terrain information, which provides new insight for a better understanding of stream sediment processes.

The use of IDW or other methods for interpolation of point data (e.g., stream sediment geochemical data) is good for rapid and convenient analysis, but interpolation of stream sediment geochemical data lacks any geomorphological and hydrodynamic considerations. Representation of stream sediment geochemical data as discrete fields, such as SCB, ESCB, WDCB and the method we propose here, takes into consideration the influence of geomorphological and hydrodynamic factors, but it can be time-consuming and can involve complex equations. For further future work, more elements (element associations) and detailed studies on the proposed method should be promoted, such as the combination of digital terrain analysis with fractal/ multifractal modeling.

6 Conclusions

Various methods of anomaly mapping have been used to analyze stream sediment geochemical data from the eastern part of the southern Gangdese metallogenic belt, including an IDW-based analysis and SCB-based analyses of MMC, 2DR, 3DR, DCR and RDCR, which were proposed to improve the traditional downstream dilution correction with the aid of digital terrain analysis. Comparison of the results of these methods in this paper led to the following conclusions:

(1) Background correction and downstream dilution correction are essential for mapping stream sediment geochemical anomalies. Therefore, although IDW (or other methods of) interpolation provides for rapid and convenient analysis of stream sediment geochemistry, geochemical anomalies mapped from continuous field representation of such data is less robust than those mapped from discrete field representations of such data.

(2) Although incorporation of analysis of geomorphological factors in the mapping of stream sediment geochemical anomalies can be complicated, digital terrain analysis provides new opportunities for a better understanding of Earth's surface processes, namely transport and deposition of stream sediments. Thus, the upslope components of stream connectivity were calculated here as a proxy for the potential for sediment produced upslope, a coefficient K being developed to adjust downstream dilution correction. Inspection of the results confirms the ability of the model that we propose and the effectiveness of the incorporation of slope effect.

(3) Further testing of the method proposed here is required in other areas with different elements, metallogenic models or geomorphic types to fully investigate its efficacy. The combination of point data interpolation and digital terrain analysis seems to be a future challenge for exploration geochemists to develop a fast, accurate and convenient method with which to map stream sediment geochemical anomalies.

Acknowledgments

This research was financially supported by the National Natural Science Foundation of China (NNSFC, Project No. 42002298), the Chinese Geological Survey (Project Nos. DD20201181, DD20211403), the National Key Research and Development Program of China (NKRDPC, Project No. 2017YFC0601501) and funded by The Project of "Big Data Analysis and Major Project Evaluation of Strategic Mineral Resources" from the Chinese Geological Survey.

Manuscript received Jan. 20, 2022
accepted Aug. 1, 2022
associate EIC: CHI Guoxiang
edited by Jeffery J. LISTON and FANG Xiang

References

Abdolmaleki, M., Mokhtari, A.R., Akbar, S., Alipour-Asll, M., and Carranza, E.J.M., 2014. Catchment basin analysis of stream sediment geochemical data: Incorporation of slope effect. Journal of Geochemical Exploration, 140: 96–103.

Afzal, P., Alghalandis, Y.F., Khakzad, A., Moarefvand, P., and Omran, N.R., 2011. Delineation of mineralization zones in porphyry Cu deposits by fractal concentration–volume modeling. Journal of Geochemical Exploration, 108: 220–232.

Ardiansyah, P.O.D., and Yokoyama, R., 2002. DEM generation method from contour lines based on the steepest slope segment chain and a monotone interpolation function. ISPRS Journal of Photogrammetry and Remote Sensing, 57: 86–101.

Ayari, J., Barbieri, M., Barhoumi, A., Belkhiria, W., Braham, A., Dhaha, F., and Charef, A., 2022. A regional-scale geochemical survey of stream sediment samples in Nappe zone, northern Tunisia: Implications for mineral exploration. Journal of Geochemical Exploration, 235: 106956.

Bonham-Carter, G.F., and Goodfellow, W.D., 1984. Autocorrelation structure of stream-sediment geochemical data: Interpretation of Zn and Pb anomalies, Nahanni River area, Yukon-Northwest Territories, Canada. Geostatistics for Natural Resources Characterization Part 2, 817–829.

Bonham-Carter, G.F., Rogers, P.J., and Ellwood, D.J., 1987. Catchment basin analysis applied to surficial geochemical data, Cobequid Highlands, Nova Scotia. Journal of Geochemical Exploration, 29: 259–278.

Borselli, L., Cassi, P., and Torri, D., 2008. Prolegomena to sediment and flow connectivity in the landscape: A GIS and field numerical assessment. Catena, 75: 268–277.

Carranza, E.J.M., 2004. Usefulness of stream order to detect

stream sediment geochemical anomalies. Geochemistry: Exploration, Environment, Analysis, 4: 341–352.
Carranza, E.J.M., 2008. Geochemical Anomaly and Mineral Prospectivity Mapping in GiS. In: Handbook of Exploration and Environmental Geochemistry, Colume 11. Amsterdam: Elsevier.
Carranza, E.J.M., 2010a. Catchment basin modelling of stream sediment anomalies revisited: Incorporation of EDA and fractal analysis. Geochemistry: Exploration, Environment, Analysis, 10: 365–381.
Carranza, E.J.M., 2010b. Mapping of anomalies in continuous and discrete fields of stream sediment geochemical landscapes. Geochemistry: Exploration, Environment, Analysis, 10: 171–187.
Carranza, E.J.M., and Hale, M., 1997. A catchment basin approach to the analysis of reconnaissance geochemical-geological data from Albay Province, Philippines. Journal of Geochemical Exploration, 60: 157–171.
Cavalli, M., and Marchi, L., 2008. Characterisation of the surface morphology of an alpine alluvial fan using airborne LiDAR. Natural Hazards and Earth System Sciences, 8: 323–333.
Cavalli, M., Trevisani, S., Comiti, F., and Marchi, L., 2013. Geomorphometric assessment of spatial sediment connectivity in small Alpine catchments. Geomorphology, 188: 31–41.
Cheng, Q., 2007. Mapping singularities with stream sediment geochemical data for prediction of undiscovered mineral deposits in Gejiu, Yunnan Province, China. Ore Geology Reviews, 32: 314–324.
Cheng, Q., 1999. Spatial and scaling modelling for geochemical anomaly separation. Journal of Geochemical Exploration, 65: 175–194.
Cheng, Q., Agterberg, F.P., and Ballantyne, S.B., 1994. The separation of geochemical anomalies from background by fractal methods. Journal of Geochemical Exploration, 51: 109 –130.
Cheng, Q., Xu, Y., and Grunsky, E., 2000. Integrated spatial and spectrum method for geochemical anomaly separation. Natural Resources Research, 9: 43–52.
Farahbakhsh, E., Chandra, R., Eslamkish, T., and Müller, R.D., 2019. Modeling geochemical anomalies of stream sediment data through a weighted drainage catchment basin method for detecting porphyry Cu-Au mineralization. Journal of Geochemical Exploration, 204: 12–32.
Ghasemzadeh, S., Maghsoudi, A., Yousefi, M., and Mihalasky, M.J., 2022. Information value-based geochemical anomaly modeling: A statistical index to generate enhanced geochemical signatures for mineral exploration targeting. Applied Geochemistry, 136: 105177.
Ghezelbash, R., Maghsoudi, A., and Carranza, E.J.M., 2019. Mapping of single- and multi-element geochemical indicators based on catchment basin analysis: Application of fractal method and unsupervised clustering models. Journal of Geochemical Exploration, 199: 90–104.
Hawkes, H.E., 1976. The downstream dilution of stream sediment anomalies. Journal of Geochemical Exploration, 6: 345–358.
He, Y., Zhou, Y., Wen, T., Zhang, S., Huang, F., Zou, X., Ma, X., and Zhu, Y., 2022. A review of machine learning in geochemistry and cosmochemistry: Method improvements and applications. Applied Geochemistry, 2022: 105273.
Kirkwood, C., Everett, P., Ferreira, A., and Lister, B., 2016. Stream sediment geochemistry as a tool for enhancing geological understanding: An overview of new data from south west England. Journal of Geochemical Exploration, 163: 28–40.
Lancianese, V., and Dinelli, E., 2015. Different spatial methods in regional geochemical mapping at high density sampling: An application on stream sediment of Romagna Apennines, Northern Italy. Journal of Geochemical Exploration, 154: 143 –155.
Leng, Q.F., Tang, J.X., and Zheng, W.B., 2016. Geochronology, geochemistry and zircon Hf isotopic compositions of the ore-bearing porphyry in the Lakang'e porphyry Cu-Mo deposit, Tibet. Earth Science, 41: 999–1015.
Li, C., Ma., T., and Shi, J., 2003. Application of a fractal method relating concentrations and distances for separation of geochemical anomalies from background. Journal of Geochemical Exploration, 77: 167–175.
Mokhtari, A.R., and Garousi Nezhad, S., 2015. A modified equation for the downstream dilution of stream sediment anomalies. Journal of Geochemical Exploration, 159: 185–193.
Morris, A.R., Anderson, F.S., Mouginis-Mark, P.J., Haldemann, A.F.C., Brooks, B.A., and Foster, J., 2008. Roughness of Hawaiian volcanic terrains. Journal of Geophysical Research Planets, 113(E12): 1–20.
Najafian, T., Mokhtari, A.R., and Albanese, S., 2020. 3D analysis of catchment basins by incorporating modified dilution correction equations in geochemical anomaly delineation. Journal of Geochemical Exploration, Elsevier B.V. doi:10.1016/j.gexplo.2020.106574.
Nforba, M.T., Egbenchung, K.A., Berinyuy, N.L., Mimba, M.E., Tangko, E.T., and Nono, G.D.K., 2022. Statistical evaluation of stream sediment geochemical data from Tchangue–Bikoui drainage system, Southern Cameroon: A regional perspective. Geology, Ecology, and Landscapes, 6(1): 1–13.
Pan, G., Wang, L., Li, R., Yuan, S., Ji, W., Yin, F., Zhang, W., and Wang, B., 2012. Tectonic evolution of the Qinghai–Tibet plateau. Journal of Asian Earth Sciences, 53: 3–14.
Parsa, M., Maghsoudi, A., Carranza, E.J.M., and Yousefi, M., 2017. Enhancement and mapping of weak multivariate stream sediment geochemical anomalies in Ahar Area, NW Iran. Natural Resources Research, 26: 443–455.
Parsa, M., Maghsoudi, A., and Yousefi, M., 2018. A receiver operating characteristics-based geochemical data fusion technique for targeting undiscovered mineral deposits. Natural Resources Research, 27: 15–28.
Qu, X., Hou, Z., Zaw, K., and Li, Y., 2007. Characteristics and genesis of Gangdese porphyry copper deposits in the southern Tibetan Plateau: Preliminary geochemical and geochronological results. Ore Geology Reviews, 31: 205–223.
Renard, K.G., Foster, G.R., Weesies, G.A., McCool, D.K., and Yoder, D.C., 1997. Predicting soil erosion by water: A guide to conservation planning with the Revised Universal Soil Loss Equation (RUSLE). United States Department of Agriculture Washington, DC.
Shahrestani, S., Mokhtari, A.R., Carranza, E.J.M., and Hosseini-Dinani, H., 2019. Comparison of efficiency of techniques for delineating uni-element anomalies from stream sediment geochemical landscapes. Journal of Geochemical Exploration, 197: 184–198.
Spadoni, M., 2006. Geochemical mapping using a geomorphologic approach based on catchments. Journal of Geochemical Exploration, 90: 183–196.
Stanley, C.R., and Sinclair, A.J., 1989. Comparison of probability plots and the gap statistic in the selection of thresholds for exploration geochemistry data. Journal of Geochemical Exploration, 32: 355–357.
Tarboron, G., 1997. A new method for the determination of flow directions and contributing area in grid digital elevation models. Water Resources Research, 33: 309–319.
Tarolli, P., 2014. High-resolution topography for understanding Earth surface processes: Opportunities and challenges. Geomorphology, 216: 295–312.
Taylor S.R., 1964. Abundance of chemical elements in the continental crust: A new table. Geochimica et Cosmochimica Acta, 28: 1273–1285.
Wang, W., Cheng, Q., Zhang, S., and Zhao, J., 2018. Anisotropic singularity: A novel way to characterize controlling effects of geological processes on mineralization. Journal of Geochemical Exploration, 189: 32–41.
Wang, W., Zhao, J., and Cheng, Q., 2014. Mapping of Fe mineralization-associated geochemical signatures using logratio transformed stream sediment geochemical data in eastern Tianshan, China. Journal of Geochemical Exploration, 141: 6–14.
Wu, B., Li, X., Yuan, F., Li, H., and Zhang, M., 2022. Transfer learning and siamese neural network based identification of geochemical anomalies for mineral exploration: A case study from the Cu-Au deposit in the NW Junggar area of northern

Xinjiang Province, China. Journal of Geochemical Exploration, 232: 106904.
Xie, X., Mu, X., and Ren, T., 1997. Geochemical mapping in China. Journal of Geochemical Exploration, 60: 99–113.
Xie, X., Wang, X., Zhang, Q., Zhou, G., Cheng, H., Lui, D., Cheng, Z., and Xu, S., 2008. Multi-scale geochemical mapping in China. Geochemistry: Exploration, Environment, Analysis, 8: 333–341.
Xiong, Y., and Zuo, R., 2022. Robust feature extraction for geochemical anomaly recognition using a stacked convolutional denoising autoencoder. Mathematical Geosciences, 54(3): 623–644.
Yousefi, M., and Carranza, E.J.M., 2015. Prediction-area (P-A) plot and C-A fractal analysis to classify and evaluate evidential maps for mineral prospectivity modeling. Computers & Geosciences, 79(C): 69–81.
Yousefi, M., Carranza, E.J.M., and Kamkar-rouhani, A., 2013. Weighted drainage catchment basin mapping of geochemical anomalies using stream sediment data for mineral potential modeling. Journal of Geochemical Exploration, 128: 88–96.
Zhang, C., Zuo, R., Xiong, Y., Zhao, X., and Zhao, K., 2022. A geologically-constrained deep learning algorithm for recognizing geochemical anomalies. Computers & Geosciences, 162: 105100.
Zuo, R., 2016. A nonlinear controlling function of geological features on magmatic-hydrothermal mineralization. Scientific Reports, 6: 1–5.
Zuo, R., 2017. Machine learning of mineralization-related geochemical anomalies: A review of potential methods. Natural Resources Research, 26: 457–464.
Zuo, R., Cheng, Q., Agterberg, F.P., and Xia, Q., 2009. Application of singularity mapping technique to identify local anomalies using stream sediment geochemical data: A case study from Gangdese, Tibet, western China. Journal of Geochemical Exploration, 101: 225–235.
Zuo, R., Wang, J., Chen, G., and Yang, M., 2015. Identification of weak anomalies: A multifractal perspective. Journal of Geochemical Exploration, 154: 200–212.
Zuo, R., Xia, Q., and Zhang, D., 2013. A comparison study of the C-A and S-A models with singularity analysis to identify geochemical anomalies in covered areas. Applied Geochemistry, 33: 165–172.
Zuo, R., and Xiong, Y., 2018. Big data analytics of identifying geochemical anomalies supported by machine learning methods. Natural Resources Research, 27: 5–13.

About the first author

XIANG Jie, male, born in 1990 in Changde, Hunan province, Ph.D., graduated from the China University of Geosciences (Beijing). Associate Professor at the International Mining Research Center, Chinese Geological Survey. Currently, he is primarily engaged in data analysis and 'Big Data'-related research. E-mail: xiangjie@mail.cgs.gov.cn.

About the corresponding author

XIA Peng, male, born in 1982 in Honghu, Hubei Province, Ph.D. candidate at the China's University of Geosciences (Wuhan). Director of Science and Technology in the Foreign Affairs Department, CGS; Director of International Mining Research Center, CGS. Currently, he is primarily engaged in resource and environmental assessment. E-mail: xiapeng@mail.cgs.gov.cn.